Simultaneous dynamic characterization of charge and structural motion during ferroelectric switching

C. Kwamen,[1] M. Rössle,[2] M. Reinhardt,[1] W. Leitenberger,[2] F. Zamponi,[2] M. Alexe,[3] and M. Bargheer[2,1,*]

[1]*Helmholtz Zentrum Berlin, Albert-Einstein-Str. 15, 12489 Berlin, Germany*

[2]*Institut für Physik & Astronomie, Universität Potsdam, Karl-Liebknecht-Str. 24-25, 14476 Potsdam, Germany*

[3]*Department of Physics, University of Warwick, Coventry CV4 7AL, United Kingdom*

(Received 4 June 2017; revised manuscript received 26 August 2017; published 10 October 2017)

Monitoring structural changes in ferroelectric thin films during electric field induced polarization switching is important for a full microscopic understanding of the coupled motion of charges, atoms, and domain walls in ferroelectric nanostructures. We combine standard ferroelectric test sequences of switching and nonswitching electrical pulses with time-resolved x-ray diffraction to investigate the structural response of a nanoscale $Pb(Zr_{0.2}Ti_{0.8})O_3$ ferroelectric oxide capacitor upon charging, discharging, and polarization reversal. We observe that a nonlinear piezoelectric response of the ferroelectric layer develops on a much longer time scale than the RC time constant of the device. The complex atomic motion during the ferroelectric polarization reversal starts with a contraction of the lattice, whereas the expansive piezoelectric response sets in after considerable charge flow due to the applied voltage pulses on the electrodes of the capacitor. Our simultaneous measurements on a working device elucidate and visualize the complex interplay of charge flow and structural motion and challenges theoretical modeling.

DOI: 10.1103/PhysRevB.96.134105

I. INTRODUCTION

Ferroelectric (FE) materials have been intensively studied since the 1930's and the first extensive review dealing with FE $BaTiO_3$ appeared already in 1950 [1]. Within the last decades, FE materials have received a revival because of their technological importance: they are not only used as capacitor dielectrics with high dielectric constant, but today's technological importance stems from the fact that FE are piezoelectric (PE), that is, they exhibit a strong coupling between externally applied electric field E and strain S [2]. An external electric field leads to an expansion or compression of the FE and vice versa. This enables to build devices that sensitively change their length due to the application of E or S results in the generation of a voltage. Typical devices are routinely used as piezoactuators, ultrasound generators, stress sensors, and many more [3].

In the last years, FE materials are believed to become materials for the development of future nonvolatile storage devices, the so-called FRAMs. These will allow to store the data bits 0 and 1 in form of the FE polarization state either pointing up or down [3]. However, the switching properties and the dynamics of FE reversal are not yet fully understood: static characterization yields a good understanding of the fundamental processes in bulk materials [4,5] but already for nanometer structures, these models have to be modified [6]. The polarization reversal involves the nucleation of domains, their growth, and movement of domain walls, which are regions separating regions with different polarization directions. Depending on the relative orientation of E and the polarization direction of the domain, a PE expansion for parallel or a compression for the antiparallel alignment is observed [7]. The commercial use of FE materials in nanometric devices requires a good understanding of the dynamics of the switching processes on a fundamental level. Up to date, there are several structural and electrical investigations of $Pb(Zr,Ti)O_3$ thin-film heterostructures with ns time resolution reported, but they typically concentrate either solely on the electrical properties [8] or the local structural response of these test devices [9].

We present in this paper the detailed simultaneous investigation of electrical and structural switching properties of a thin $Pb(Zr_{0.8}Ti_{0.2})O_3$ (PZT) test structure with a time resolution of ∼2 ns. The high time resolution of the complementary information from the electrical and structural properties allows us to investigate the dynamics of the FE reversal process after application of an electrical switching pulse and follow the different steps during the polarization reversal of the FE.

II. EXPERIMENT

In this study, we use time-resolved reciprocal space mapping (tr-RSM) to measure the structural dynamics in a PZT thin-film capacitor while it undergoes a standard ferroelectric test cycle. We selected a large area capacitor with a rather slow RC time constant of $\tau_{RC} = 1\ \mu s$ for charging and discharging. The device consists of a ∼250 nm thick PZT film, grown by pulsed laser deposition on a ∼50 nm thick metallic $SrRuO_3$ bottom electrode [10]. The substrate is (001) oriented $SrTiO_3$. In order to apply the electrical field across the PZT film, we use ∼20 nm thick Pt electrodes of hexagonal shape with 0.3 mm edge length and 0.5 mm diameter. These are contacted from top with a W needle. The device and experimental geometry are schematically shown in Fig. 1(a). We probe the structural response with x rays incident through the Pt electrode as we apply voltage pulses up to $U = \pm 8$ V with varying length and shape with a HP33120A pulse generator. We restricted ourselves to voltages well below the damage threshold of ∼10 V and measured the resulting current signal via the 50 Ω resistance of an oscilloscope (Agilent DSO9404A). The typical hysteresis loop of such a FE capacitor device is shown in Fig. 1(b) for $U = \pm 8$ V and a frequency of 4 KHz. We display the measured current trace and the calculated

*bargheer@uni-potsdam.de

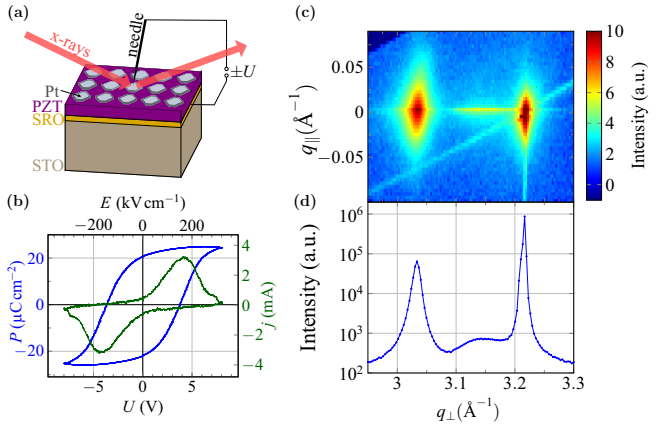

FIG. 1. Device structure and characterization. (a) Sample structure showing the stacking sequence of the different layers, connections to the external bias, and direction of the x-ray beam. (b) Polarization P, electric field E hysteresis loop, and switching current j recorded at 4 kHz. (c) Typical RSM around the 002 Bragg reflections of PZT, $SrRuO_3$, and $SrTiO_3$ of the as-grown film and (d) line profile obtained from panel (c) at $q_\parallel = 0$.

polarization P as function of the applied bias voltage U. Our measurements at the synchrotron yield a rather low polarization value of $P_S = 25\ \mu C/cm^2$, which is by a factor of 3 lower as compared to complementary measurements on the same sample [11] and other comparable samples [10]. We attribute this to the high contact resistance between needle and electrode, but this virtual reduction does not affect our conclusions as they do not rely on the absolute measured values of the sample polarization.

For the electrical characterization and device switching, we apply the so-called PUND test scheme, where we apply two *p*ositive *u*p pulses followed by two *n*egative *d*own pulses [12,13]. This allows us to separate the charging response of the device from the FE switching response. We obtain the FE response by subtracting the second nonswitching pulse response from the first one: the first pulse charges the capacitor and reverses its polarity and with the second pulse we probe only the charging as the device is already polarized in the direction given by the polarity of the external field. The nonswitching pulse triggers a PE response associated with domain-wall motion. The two following pulses repeat the analysis with opposite polarity. During the applied electrical bias voltage, we record the current $j(t)$ from which we obtain the charge $Q(t)$ after integration of $j(t)$ over t.

The structural response as function of time and bias field of the device was measured at the XPP-KMC3 end station of the synchrotron BESSY II, Berlin, Germany. A 200 μm wide monochromatic x-ray beam with 9 keV photon energy was aligned to one Pt electrode in Bragg geometry with help of the four circle goniometer installed at the beamline. The diffracted x rays were detected with a two-dimensional detector (Pilatus 100k, Dectris). We record the symmetrically and asymmetrically scattered x rays with the two-dimensional pixel detector for various angles ω between the incoming x rays and the sample surface [14]. A unitary transformation maps this signal onto the scattering intensities [15,16] shown as a function of the reciprocal space coordinates parallel and perpendicular to the sample surface, $q_\parallel$ and $q_\perp$ in Fig. 1(c). As we are interested in the dynamics of the polarization switching process of PZT, we synchronized the detector to the first rising edge of the electrical PUND sequence. This allows us to retrieve the reciprocal space map for different times t. However, the gate window for the Pilatus detector of 100 ns limits the time resolution and we can only use a fraction of the x-ray flux. Thus, some experiments were performed with a fast x-ray scintillator together with a photomultiplier tube (Hamamatsu). This device is operated in single-photon counting mode and we can use the full x-ray flux [17]. We correlate the photon counts to the pulse sequence with a single-photon counting module (PicoHarp 300, PicoQuant). This allows us to follow the sequence of electrical and structural events taking place during the polarization reversal with a time resolution of 2 ns. With the photomultiplier we obtained ω scans that reproduce the line profile extracted from the RSM at $q_\parallel = 0$ and which is shown in Fig. 1(d). We identify in the RSM and the line profile the 002 Bragg reflections of PZT, the $SrRuO_3$ bottom electrode, and the $SrTiO_3$ substrate. From the $SrRuO_3$ bottom electrode we only see a very broad streak as the film is very thin. The $SrTiO_3$ substrate reflection is sharp and intense. Our sample does not exhibit a significant amount of a domains of the PZT film, which would appear as additional Bragg reflection between the PZT and the $SrTiO_3$ substrate reflections [18]. From this measurement we estimate the volume fraction of a domains to be less then 5% in our sample, which is in agreement with samples grown under comparable conditions [10] and does not change with the increasing number of switching cycles. We have also not observed a strong variation of the volume fraction at other investigated Pt electrodes (not shown here). The leakage current has been demonstrated to depend on the electrode material and Pt exhibits the best device performance values [19]. We have measured typically 10^8 switching cycles on an electrode but have experienced device failure earlier (10^6), especially at higher bias voltages, but also extended lifetimes of the device up to 10^9 switching cycles but have not systematically investigated this. The experimental data shown in Figs. 2–4 are typically averaged for 1 h of measurement time, which amounts to more than 7×10^6 reversible switching cycles at a frequency of 2 kHz.

III. RESULTS AND DISCUSSION

Our experiment allows us to determine the sequence of electrical and structural events taking place during the polarization reversal of the FE. We first present the structural information deduced from tr-RSM and the simultaneously recorded electrical measurement using a rectangular PUND sequence. Figure 2 summarizes all the simultaneously measured electrical and structural responses to the applied rectangular PUND sequence indicated in Fig. 2(a). For compactness of the representation in all panels, red lines encode the positive bias corresponding to the upper horizontal time axis and blue lines encode negative bias pulses corresponding to the lower horizontal time axis.

The measured current $j(t)$ in Fig. 2(b) rises and decays within $\tau_{RC} = 1\ \mu s$ as a response to the nonswitching pulses. The response to the switching pulses exhibits an additional current due to FE switching that decays on a time scale of

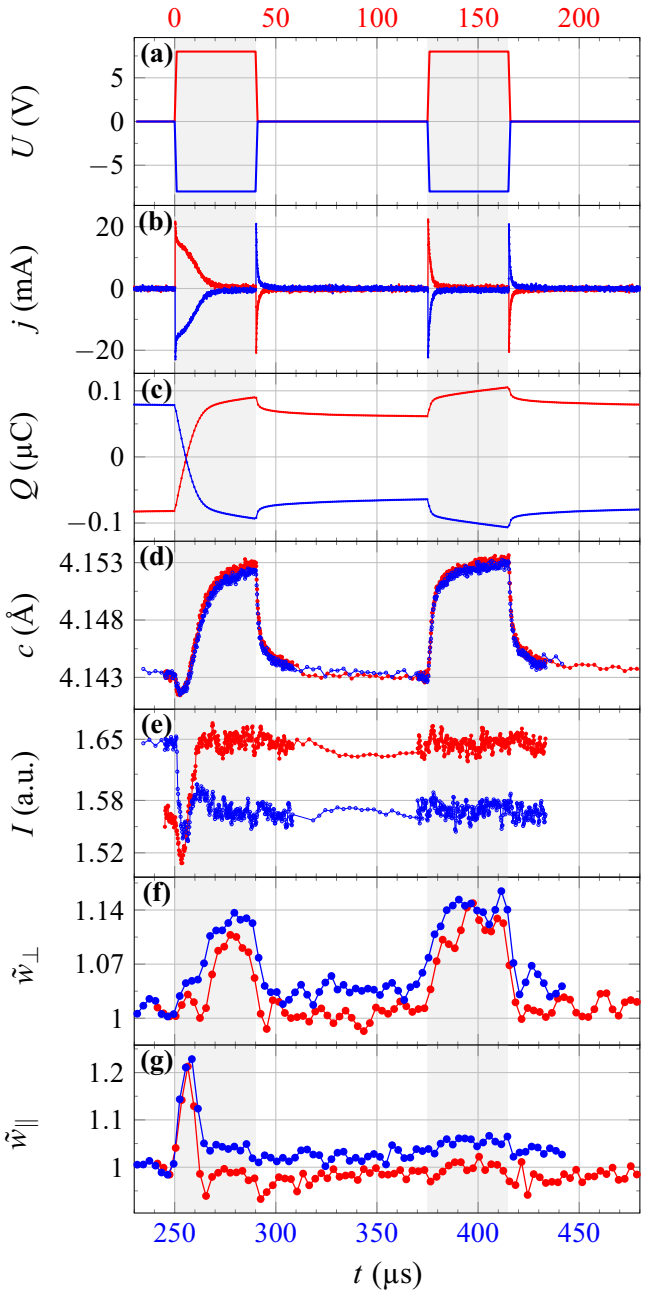

FIG. 2. Device response to the applied rectangular PUND sequence. The red color represents positive bias and the blue color encodes negative bias. (a) Applied PUND voltage sequence $U(t)$. (b) Measured current response $j(t)$. (c) Corresponding charge $Q(t)$ obtained after integrating the current signal in (b) over time. (d) Out-of-plane lattice constant $c(t)$. (e) Integrated intensity $I(t)$. (f) Normalized FWHM of the out-of-plane Bragg peak $\tilde{w}_\perp(t)$. (g) Normalized FWHM of the corresponding scattering vector parallel to film surface $\tilde{w}_\parallel(t)$.

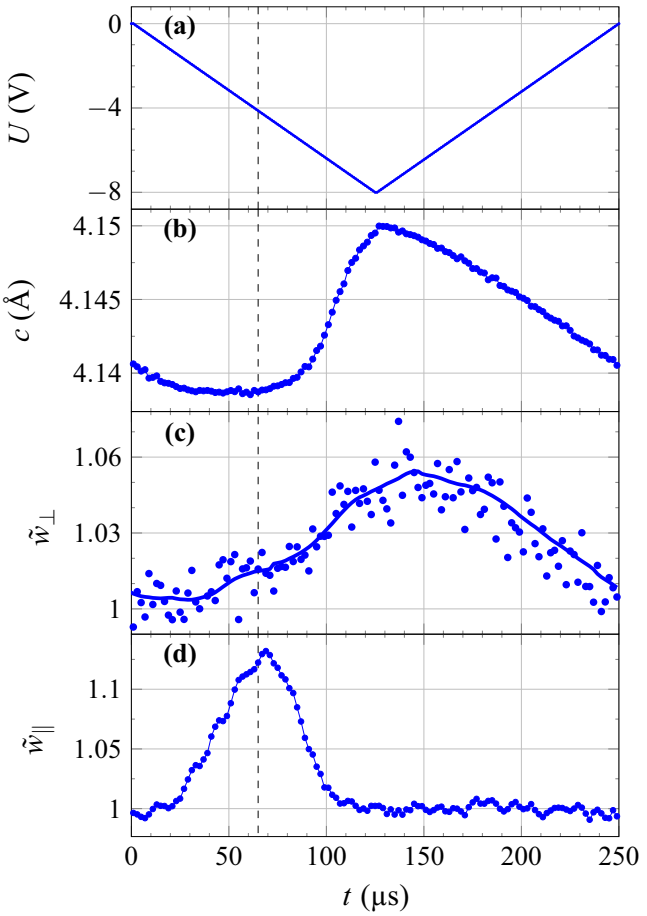

FIG. 3. Switching dynamics of PZT due to a triangular voltage ramp. (a) First half of the applied voltage pulse pattern $U(t)$. (b) Out-of-plane lattice constant $c(t)$. (c) Normalized FWHM $\tilde{w}_\perp$ of the out-of-plane Bragg peak and (d) normalized FWHM $\tilde{w}_\parallel$ of the in-plane component.

$\sim$20 μs. Hence, we chose the pulse length of 40 μs and the repetition rate of 2 kHz according to the duty cycle of the device. Figure 2(c) shows the charge $Q(t)$ of the capacitor at positive and negative bias, respectively. Voltage, current, and charge [Figs. 2(a)–2(c)] show mirror images for the positive and negative bias, that is, the device is essentially symmetric despite the different top and bottom electrode materials. The time-resolved Bragg-peak shift of the 002 Bragg reflection of PZT reveals the changes of the out-of-plane lattice constant $c(t) = 2\pi/q_\perp^{(002)}(t)$ in Fig. 2(d), which resemble each other for positive and negative bias: the nonswitching pulses yield an expansion of the lattice. During the switching pulses, in contrast, we observe a small compression of the lattice right after application of the bias voltage. The integrated peak intensity $I(t)$ in Fig. 2(e) shows a clear change of about 5% upon switching of the device. We remind here that the integrated peak intensity $I(t) \propto |F(t)|^2$ [20], hence, we obtain a quantity that is proportional to the square of the structure factor $|F|$. The peak intensity is larger after switching the device with a positively charged Pt electrode. During the short time, where the lattice compression is observed in Fig. 2(d), the peak intensity is also transiently suppressed by additional 3% within $\sim$1 μs whereas the current reaches its maximum after $\sim$4 μs. The peak widths $\tilde{w}_\perp(t) = w_\perp(t)/w_\perp(t=0)$ along $q_\perp$ perpendicular to the film [Fig. 2(f)] and $\tilde{w}_\parallel(t) = w_\parallel(t)/w_\parallel(t=0)$ along $q_\parallel$, parallel to the film plane [Fig. 2(g)], increase during the switching pulses. However, only $\tilde{w}_\perp(t)$ increases during nonswitching pulses. $\tilde{w}_\parallel$ is only increased in the first 10 μs of the switching pulses whereas $\tilde{w}_\perp$ responds after $\tilde{w}_\parallel$ has already returned to its initial value.

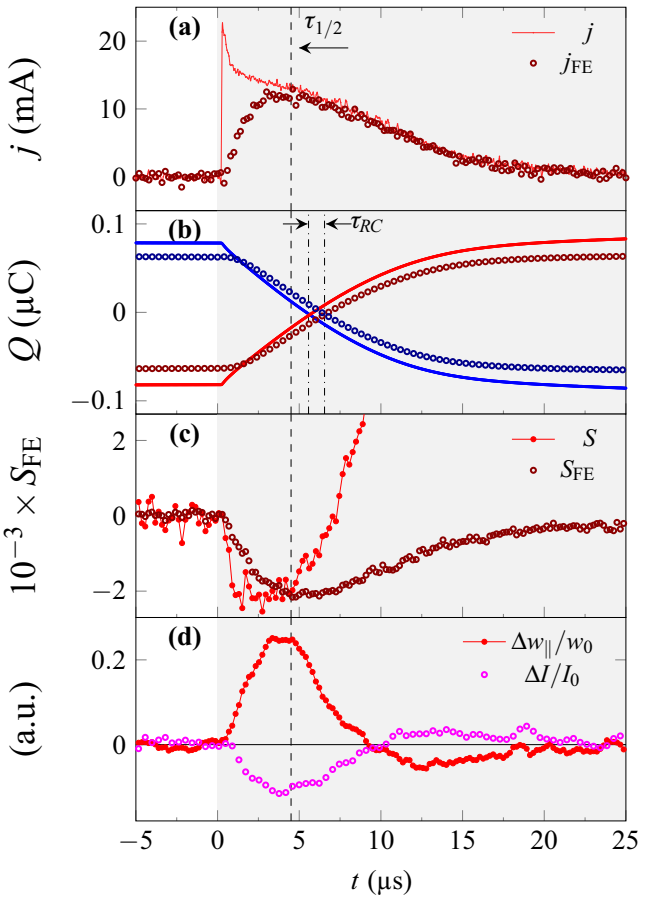

FIG. 4. Sequence of events during polarization reversal. (a) Current $j(t)$ (solid red line) as measured during the polarization reversal plotted together with the current $j_{FE}(t)$ due to the FE switching. (b) The calculated charges $Q(t)$ (solid lines) and $Q_{FE}(t)$ (symbols) associated to the FE switching. (c) The strain $S(t)$ (filled red circles) as measured compared to the strain due to the FE polarization reversal (open symbols). (d) Transient intensity reduction $\Delta I(t)/I(t=0)$ and transient width increase $\Delta w_{\parallel}(t)/w_{\parallel}(t=0)$. For the definition of the symbols, see main text. The dashed vertical line indicates $\tau_{1/2}$, the time after which 50% of the sample has been reversed. This time coincides with the observed maximum of j_{FE}, the beginning of the rise of the expansive strain $S(t)$, the minimum of S_{FE}, and the minimum of the transient intensity reduction. Note that the compensation time of the charges $\tau_{1/2}$ lags behind by τ_{RC}.

Now, we discuss the capacitive and PE response of the film upon the nonswitching pulses. Looking at the charging and discharging current spikes in Fig. 2(b), we can fit an exponential decay with the time constant $\tau_{RC} = 1\ \mu$s to the signal. In Fig. 2(c) the continuous rise of the charge might at first be attributed to a leakage current, however, Fig. 2(d) clearly shows that during the 40 μs time scale the PE strain keeps rising. The constant bias voltage sets the external electric field in the FE. Therefore, the slow additional PE response that we observe when the external voltage is constant, especially also while the external voltage is switched off, must be ascribed to a slow structural relaxation such as domain-wall creep motion or pinning. This slow component of charge flow is not given by the electronic time scale τ_{RC}. These charges slowly flow in addition because the structural relaxation is connected to charge flow by the piezoelectric structure given by the cations and the oxygen octahedron. This accounts for the slow increase and decrease of $Q(t)$ in Fig. 2(c). We note that during this process $\tilde{w}_{\parallel}$ in Fig. 2(g) is constant as this slow process only switches those 10% of the total polarization that accounts for the difference in the saturation polarization P_S to the remanent polarization P_R. The increase of $\tilde{w}_{\perp}$ indicates inhomogeneities in the PE response across the whole electrode area [9]. Due to the additional increase of $Q(t)$, the internal field in the FE is not constant. This manifests in the PE coefficient d_{33} that is evidently not constant on such short time scales. This is not a contradiction to the static situation where d_{33} is constant. It has been shown that the PE response might exhibit nonstatic and nonlinear contributions [21–23].

The structural response during the polarization reversal has microscopic and mesoscopic components. The peak intensity shown in Fig. 2(e) is higher for positive bias. According to the commonly accepted structural model, the Ti atom is guided by the surrounding O octahedra in the same direction, i.e., the positively charged Ti moves towards the positive electrode, albeit less than the apical O. We calculate a ∼7% structure factor change for the switching from 002 to 00$\bar{2}$ [11,24] due to the violation of Friedel's law [20,25,26]. The higher intensity is obtained for the O octahedra moved towards the positively charged Pt electrode through which the x rays are incident. This static structural model is confirmed by our data for times $t > 20\ \mu$s, when the polarization reversal is essentially completed. For the early times $t < 20\ \mu$s we observe for both polarities in Fig. 2(e) the additional decrease in intensity by 3%. This may be ascribed to a transient structural disorder in the position of the Ti atom and the O octahedra analogous to the thermal disorder described by the Debye-Waller effect. At the same time, the in-plane peak width $\tilde{w}_{\parallel}$ transiently increases. This must be attributed to a loss of in-plane coherence of the lattice, i.e., domain formation. When $\tilde{w}_{\parallel}$ relaxes around $t \approx 20\ \mu$s, the out-of-plane peak width $\tilde{w}_{\perp}$ rises to the same value as during the nonswitching pulse. Therefore, the changes $\tilde{w}_{\perp}$ in the out-of-plane peak width are attributed to different peak strain values attained across an inhomogeneous large electrode. For $t < 20\ \mu$s, the peak width increase $\tilde{w}_{\perp}$ is not yet fully developed. At first one would expect a maximum difference in the expansive and compressive strain for the two domain orientations that exist during the switching process because they have PE coefficients with opposite sign [27]. We see two reasons for our unexpected observation of an initially reduced $\tilde{w}_{\perp}$ along c: structural clamping of domains and insufficient screening. As long as the needlelike domains emerging from nucleation sites are laterally small, the lattice constant is clamped to the adjacent domain that experiences strain with opposite sign. For small domain sizes, the oppositely poled domains hinder each other's expansion. Second, during the ferroelectric switching, the screening of the switched ferroelectric dipoles by charges on the electrode lags behind the structural response by τ_{RC}, leading to effectively reduced field inside the capacitor as we will show in the following.

In order to confirm our conclusions and to highlight the timing of the structural response during the switching, we carefully investigated the effect of a triangular voltage ramp. We

show in Fig. 3 only the negative part, which is one half of the cycle used to measure the hysteresis loop presented in Fig. 1(b).

Starting at the pulse onset at $t = 0$, the lattice constant in Fig. 3(b) shows a small gradual reduction confirming the compressive PE response in the initial stage of the switching. When the field in the film reaches $E \approx 165$ kV/cm ($U = 4.1$ V), the lattice constant reaches its minimum value $c_{\min}$ and subsequently exhibits a rapid and strong expansion. The maximum compression at $c_{\min}$ is larger for the triangular pulse compared to the rectangular PUND sequence shown in Fig. 2. At first, one would expect it to be smaller because the applied voltage is smaller ($U = 4.1$ V in contrast to 8 V) at the time $\tau_{\min}$ marked by the vertical dashed line in Fig. 3. In addition, the slowly rising field should give the film more time to reverse the polarization. We therefore conclude that the fast application of the external field during the PUND sequence leads to an increased depolarization field associated with the already switched domains. This field is not yet fully screened because the charges on the electrodes lag behind the structural changes, explaining the rather small compressive PE response during the rectangular pulse. The peak width increase $\tilde{w}_\perp$ along $q_\perp$ in Fig. 3(c) mimics the response of the PE expansion after the coercive field is surpassed. In contrast, $\tilde{w}_\parallel$ in Fig. 3(d) increases already at very small fields, reaches a maximum near the coercive field at $\tau_{\min}$, and then rapidly decreases. The expanded FE film almost linearly recovers as the voltage is reduced linearly and reaches finally its initial value. This implies a constant PE coefficient d_{33} after the switching has occurred, which is the same as the steady-state value.

In order to confirm our conclusions about the incomplete screening during the polarization reversal, we show in Fig. 4 the simultaneously collected information at the onset of the switching pulse of the PUND sequence. In Fig. 4(a) we show the measured switching current $j(t)$, which rises quasi-instantaneously after the application of the external bias. In Fig. 4(a) we also include the current $j_{\rm FE}(t)$ associated with the FE switching, which we obtain as the difference $j_{\rm FE}(t) = j(t) - j_{\rm PE}(t)$ between the switching and nonswitching current transients. From these traces we calculate the corresponding charges $Q(t)$ (solid lines) and $Q_{\rm FE}$ (symbols), which we show in Fig. 4(b). As soon as the charges appear on the electrodes, the electric field in the capacitor equals $E = U/d$. Since in the beginning of the switching pulse the elementary dipoles of the FE are pointing in the opposite directions, a compressive strain develops at the same rate at which the expansion increases during the applied field at the nonswitching pulses. However, this compression already stops after ~ 1 μs, although only a very small fraction of less than 5% of the crystal has according to the measured charge in 4(b) been switched. The screening of these charges associated to the FE reversal lags behind the structural response: the crossing of $Q_{\rm FE}$ occurs delayed by τ_{RC} with respect to the compensation point of the total Q. This partially cancels the applied external electric field, explaining why the amplitude of the compression is five times smaller than the following expansion. This is consistent with the reduction of the Bragg peak intensity, as a weaker field imposes a less strict ordering of the atomic positions. In Fig. 4(c) we show the transient strain $S = c(t)/c(t = 0) - 1$, as obtained from the measurement (red line) together with the transient strain $S_{\rm FE}$ (brown symbols) that we have obtained from the subtraction of the nonswitching pulse contribution from the switching pulse. From the difference of both transients we see that the minimum strain due to the external field appears earlier than the compression due to the polarization reversal. We assign the point where the minimum strain due to the FE switching appears and at the same time the overall compression of the PZT layer stops as the time $\tau_{1/2}$ where half of the sample has been switched, that is, the PE compression turns into an expansion. This is consistent with the observed transient minimum of the peak intensity $\Delta I(t)/I(t = 0) = [(I^+(t) + I^-(t))/I(t = 0)] - 1$ as response to the structural disorder displayed in Fig. 4(d). The corresponding transient width change $\Delta w_\parallel(t)/w_\parallel(t = 0) = w_\parallel(t)/w_\parallel(t = 0) - 1$ starts at $\tau_{1/2}$ to decrease, indicating that structurally the switching is finished and only the PE expansion contributes to the observed transient strain. Note that also the onset of the disorder and the onset of $j_{\rm FE}$ lag behind the minimum of the PE contraction. In other words, the disorder and the FE switching current proceed while the potential barrier between both polarization states is suppressed by the compressive strain in the domains that are not yet switched. For the observed compressive strain of $\Delta c(t_{\min})/c(t = 0) = 4 \times 10^{-4}$ and expansive strain $\Delta c(t_{\max})/c(t = 0) = 2 \times 10^{-3}$ we estimate the modulation of the potential barrier to be 1 to 5 meV, based on *ab initio* calculations that predict a barrier suppression from 0.23 eV for a tetragonal distortion $c/a = 1.06$ to 0.1 eV for $c/a = 1$ [28]. We quantify from this transient reduction of the potential barrier that the charge imbalance and the resulting strain are the driving force for the polarization reversal of the PZT FE device.

IV. CONCLUSIONS

In conclusion, we have simultaneously observed the charge flow and the structural motion during FE polarization reversal of a PZT test device. We find charge flow connected to domain-wall motion during the structural relaxation of the piezoelectric crystal structure. The field induced switching events start with a short piezoelectric compression which is about five times smaller than the following piezoelectric expansion observed after the polarization reversal. During the switching process, the depolarization field of the already switched dipoles is not yet completely screened by the external charges on the electrodes. The strain due to the piezoresponse modulates the energy barrier between up and down polarization states and supports the polarization reversal. We believe that the experimental results found by simultaneous assessment of the structural and electronic response of this prototype FE capacitor will be useful in devising new concepts for FE polarization reversal and understanding the combined electromechanical response of ferroelectrics. Future experiments shall, e.g., monitor the ultrafast charge flow in a biased device which is compressed by a hypersound wave to reduce the energy barrier.

ACKNOWLEDGMENTS

M.A. acknowledges the financial support of Royal Society through Wolfson Research Merit and Theo Murphy Blue Sky Awards. C.K. would like to thank Q. Cui and W. Wirges for help with the ferroelectric test cycles.

[1] A. von Hippel, Rev. Mod. Phys. **22**, 221 (1950).

[2] H. F. Tiersten, J. Acoust. Soc. Am. **70**, 1567 (1981).

[3] N. Setter, D. Damjanovic, L. Eng, G. Fox, S. Gevorgian, S. Hong, A. Kingon, H. Kohlstedt, N. Y. Park, G. B. Stephenson *et al.*, J. Appl. Phys. **100**, 051606 (2006).

[4] E. Fatuzzo, Phys. Rev. **127**, 1999 (1962).

[5] J. F. Scott, Ferroelectrics **503**, 117 (2016).

[6] A. K. Tagantsev, I. Stolichnov, N. Setter, J. S. Cross, and M. Tsukada, Phys. Rev. B **66**, 214109 (2002).

[7] D.-H. Do, A. Grigoriev, D. M. Kim, C.-B. Eom, P. G. Evans, and E. M. Dufresne, Integr. Ferroelectr. **101**, 174 (2008).

[8] J. F. Scott, L. Kammerdiner, M. Parris, S. Traynor, V. Ottenbacher, A. Shawabkeh, and W. F. Oliver, J. Appl. Phys. **64**, 787 (1988).

[9] A. Grigoriev, D.-H. Do, D. M. Kim, C.-B. Eom, B. Adams, E. M. Dufresne, and P. G. Evans, Phys. Rev. Lett. **96**, 187601 (2006).

[10] I. Vrejoiu, G. L. Rhun, L. Pintilie, D. Hesse, M. Alexe, and U. Gösele, Adv. Mater. **18**, 1657 (2006).

[11] We have measured the E-P hysteresis loop with a home-built Sawyer tower and compared these results to PUND sequences with triangular and rectangular pulses. We obtained in our laboratory a value of $P_S \approx 70\ \mu C/cm^2$.

[12] S. D. Traynor, T. D. Hadnagy, and L. Kammerdiner, Integr. Ferroelectr. **16**, 63 (1997).

[13] I. Fina, L. Fàbrega, E. Langenberg, X. Martí, F. Sánchez, M. Varela, and J. Fontcuberta, J. Appl. Phys. **109**, 074105 (2011).

[14] V. Holy, U. Pietsch, and T. Baumbach, *High-resolution X-ray Scattering from Thin Films and Multilayers* (Springer, Berlin, 2006).

[15] D. Schick, A. Bojahr, M. Herzog, P. Gaal, I. Vrejoiu, and M. Bargheer, Phys. Rev. Lett. **110**, 095502 (2013).

[16] D. Schick, R. Shayduk, A. Bojahr, M. Herzog, C. Von Korff Schmising, P. Gaal, and M. Bargheer, J. Appl. Crystallogr. **46**, 1372 (2013).

[17] H. Navirian, R. Shayduk, W. Leitenberger, J. Goldshteyn, P. Gaal, and M. Bargheer, Rev. Sci. Instrum. **83**, 063303 (2012).

[18] H. A. Navirian, D. Schick, P. Gaal, W. Leitenberger, R. Shayduk, and M. Bargheer, Appl. Phys. Lett. **104**, 021906 (2014).

[19] L. Pintilie, I. Vrejoiu, D. Hesse, and M. Alexe, J. Appl. Phys. **104**, 114101 (2008).

[20] J. Als-Nielsen and D. McMorrow, *Elements of Modern X-ray Physics*, 2nd ed. (Wiley, Hoboken, NJ, 2011).

[21] D. Damjanovic, J. Appl. Phys. **82**, 1788 (1997).

[22] S. Trolier-McKinstry, N. Bassiri Gharb, and D. Damjanovic, Appl. Phys. Lett. **88**, 202901 (2006).

[23] A. Grigoriev, R. Sichel, H. N. Lee, E. C. Landahl, B. Adams, E. M. Dufresne, and P. G. Evans, Phys. Rev. Lett. **100**, 027604 (2008).

[24] B. Noheda, J. A. Gonzalo, L. E. Cross, R. Guo, S.-E. Park, D. E. Cox, and G. Shirane, Phys. Rev. B **61**, 8687 (2000).

[25] S. Gorfman, H. Simons, T. Iamsasri, S. Prasertpalichat, D. P. Cann, H. Choe, U. Pietsch, Y. Watier, and J. L. Jones, Sci. Rep. **6**, 20829 (2016).

[26] We calculate a much smaller structure factor change at 9 keV than is experimentally observed in Ref. [9] at 10 keV. Grigoriev *et al.* use a highly focused x-ray beam of 115 nm width and hence probe only a very small fraction of the sample. The penetration depth of the x rays is significantly increased at 10 keV.

[27] We note that the sign of d_{33} has to change at the coercive field as it is required for FE polarization reversal.

[28] R. Cohen, Nature (London) **358**, 136 (1992).